Editors' Suggestion

Topological Edge States in Quasiperiodic Locally Resonant Metastructures

Yiwei Xia,[1,*] Alper Erturk,[1] and Massimo Ruzzene[2]

[1] *George W. Woodruff School of Mechanical Engineering, Georgia Institute of Technology, Atlanta 30332, USA*
[2] *Department of Mechanical Engineering, University of Colorado Boulder, Boulder 80309, USA*

(Received 3 September 2019; revised manuscript received 5 December 2019; published 14 January 2020)

We investigate the dynamic behavior and topology of quasiperiodic resonant metastructures. We show that the quasiperiodic arrangement of resonators introduces frequency band gaps in addition to the locally resonant band gap defined by the natural frequency of the resonators. The concept is illustrated on a beam with an array of mechanical resonators. Numerical evaluation of the spectrum as a function of the quasiperiodic arrangement of resonators reveals a structure reminiscent of a Hofstadter butterfly and allows the study of key topological properties. The results illustrate the occurrence of additional band gaps that are topologically nontrivial and that host edge-localized modes in finite structures. The occurrence of these gaps and of the associated edge states is demonstrated experimentally by measuring the frequency response of the beam and by evaluating the spatial distribution of selected operational deflection shapes. The results unveil the potential of deterministic quasiperiodic structural designs to induce wave localization and attenuation over multiple frequency bands, which may find applications in vibration isolation and energy harvesting, among others.

DOI: 10.1103/PhysRevApplied.13.014023

I. INTRODUCTION

Locally resonant (LR) metamaterials and metastructures have been broadly investigated in recent decades. Theoretical and numerical studies have shown that linear local resonators produce subwavelength frequency band gaps that enable low-frequency attenuation of sound and vibrations [1–7]. Most investigations have considered nominally identical resonators that are regularly, or periodically, placed within the structure. In these cases, the LR band-gap center frequency is defined through the natural frequency of the resonators, while its width is mostly determined by the added inertia [7]. Attempts at extending the resonant gap through nonuniform resonators, both in terms of their natural frequency and of their spacing, can be found in Refs. [3,8,9], among others. Parallel to these efforts, there is considerable interest in the conditions that govern the onset of localization [10–12]. Vibration localization can be beneficial both in terms of isolating components and limiting exposure but can also be the source of catastrophic failures [13] and therefore is of great relevance to the engineering community.

Inspired by the discovery of topologically nontrivial phases in electronic [14] and photonic [15] systems, various classes of topological phenomena such as quantum Hall and quantum spin Hall effects have been studied and realized in acoustic and mechanical systems [16]. These works exploit defect-immune modes localized at edges or interfaces for robust acoustic and/or elastic waveguiding. Recently, topological phases have also been explored in lower-physical-dimensional systems by exploiting virtual dimensions in relevant parameter spaces [17–20]. In particular, quasicrystalline or quasiperiodic structures have been linked to topological insulators [21–23]. Quasiperiodicity defines a broad class of geometrical patterns, of which periodic assemblies are particular cases. Thus, the study of quasiperiodic (QP) arrangements of inclusions can extend the range of capabilities of periodic metamaterials and metastructures [24].

A recent line of work considers a framework to investigate QP systems based on the evaluation of their spectral properties, the evaluation of the density of states, and the estimation of topological invariants that may characterize nontrivial gaps and the onset of associated edge states [25–28]. For example, recent work in mechanics [25] has demonstrated that topological boundary modes can emerge solely from the patterning of a metamaterial, in a manner that is entirely independent of the structure of the resonators and their coupling. The experimental observations in Ref. [25] also show the onset of localized modes at the boundary of finite arrays of discrete mechanical resonators, implemented in the form of a chain of magnetically coupled spinners. Topological boundary and interface modes in QP acoustic waveguides are also observed in Ref. [26], while reconfigurable QP acoustic crystals [27] are employed to experimentally observe their spectrum in

*yxia63@gatech.edu

the form of a Hofstadter butterfly [29]. Furthermore, the numerical results in Ref. [28] have shown how a Hofstadter spectrum also characterizes continuous structural beams supported by a QP array of ground springs and how localized modes can be predicted through topological considerations on such a spectrum. The studies referenced above provide insights into modes that are localized at edges or interfaces and suggest new methodologies for wave transport and localization. Also, this body of work generally contributes to the literature that regards QP geometries as projections of higher-dimensional manifolds onto lower-dimensional lattices and that explores topological properties of higher-dimensional periodic systems, to assess properties in the lower-dimensional physical space.

II. QUASIPERIODIC PATTERN GENERATION

Motivated by previous contributions, here we investigate a LR beam with QP distributions of resonators. Extending the results in Ref. [28], we consider elastic beams in transverse motion equipped with local resonators located at positions defined by the projection operation described in Ref. [25]. This pattern-generating procedure identifies families of structures ranging from periodic to QP obtained through smooth variation of the parameters defining the projection, which can be interpreted geometrically as shown in Fig. 1. Accordingly, the location of resonator s is given by

$$x_s = sa + R\sin(2\pi s\theta). \tag{1}$$

Here, a is the distance between the centers of adjacent circles defining the spacing between resonators in an underlying periodic arrangement, while the radius of the circle $R < a/2$ and the angular increment θ define the projection. The rational and irrational θ values define periodic and QP patterns, respectively. For $\theta = 0$, the system has a periodicity of a and the resonators are placed uniformly on the beam. For rational $\theta = p/q$ (p and q are coprime integers), the system has a periodicity of qa. In contrast, no periodicity or translational symmetry exists for irrational θ values. In addition, all resonators are here assumed to have the same mass m and stiffness k. The governing equations

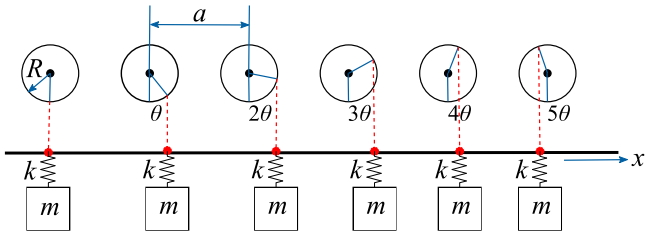

FIG. 1. The projection operation for placement of the local resonators according to the procedure described in Ref. [25]).

for the beam and the sth resonator are

$$D\frac{\partial^4 w(x,t)}{\partial x^4} + \rho A\frac{\partial^2 w(x,t)}{\partial t^2} - k\sum_s w_s(t)\delta(x - x_s) = 0, \tag{2}$$

$$m\frac{\partial^2[w(x_s,t) + w_s(t)]}{\partial t^2} + kw_s(t) = 0, \tag{3}$$

where $w(x,t)$ is the transverse displacement of the beam and $w_s(t)$ is the displacement of the sth resonator relative to the beam. Also, $D = EI$ is the beam bending stiffness, where E is the Young's modulus, and I is the second moment of area of the beam cross section, while ρ is the density and A is the cross-section area. We consider an aluminum beam (mass density $\rho = 2700$ kg/m^3, Young's modulus $E = 69$ GPa) of cross section 0.8×25.2 mm^2. All resonators have a natural frequency of 90 Hz and the added-mass ratio is 1.26. The added-mass ratio is defined here as the ratio of the total mass of added resonators to the mass of the plain beam without resonators. In addition, $a = 5.08$ cm and $R = 0.3a$ are chosen as fixed dimensions in accordance with the considered experimental setup described below.

III. TOPOLOGICAL BAND GAPS AND EDGE-LOCALIZED STATES

The study is conducted in terms of variations in θ, which is the considered free QP parameter. We first evaluate the spectrum of an infinite beam, which is approximated by considering all rational values of θ that are commensurate with $S = 600$ cells. Periodic boundary conditions are imposed on both ends of the beam, so that it geometrically resembles a ring (for details, refer to Ref. [28]). Employing an analysis approach based on Galerkin's approximation [28], we evaluate the resonant frequencies for all configurations ($\theta = s/S$, $s = 1, 2, \ldots, S$) and plot them to obtain the approximated bulk spectrum shown in black in Fig. 2(a). The resonant frequencies of the ring discretize the bulk spectrum. The density of the discretization increases as the number of unit cells S increases. Variation of vibrational frequencies in terms of the QP parameter leads to a pattern that is reminiscent of the Hofstadter butterfly [29]. In addition, estimating the spectral properties of a finite simply supported beam of length $L = aS$, including $S = 30$ unit cells, leads to the finite-structure frequencies denoted by the red dots in Fig. 2(a). Both the bulk and the finite spectra are characterized by a LR band gap that is topologically trivial, as demonstrated by the fact that it remains constant as θ varies. Depending on the boundary conditions of the finite structure, the modes localized at the edge may or may not appear inside the LR band gap. This gap separates two spectral regions, which feature several additional band gaps the center frequencies and widths of which depend on the value of θ. These additional

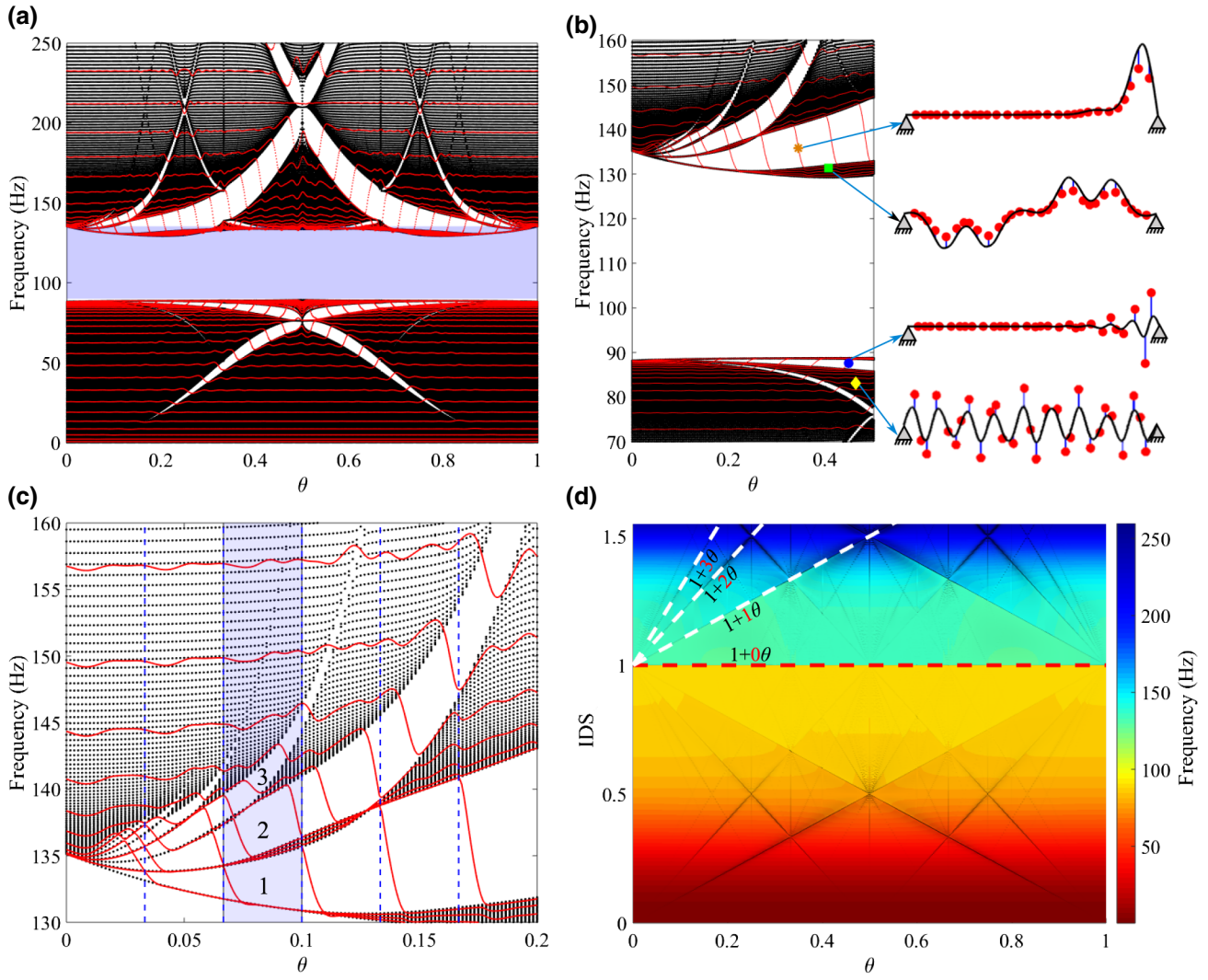

FIG. 2. (a) Bulk (black) and finite-beam (red) spectra as a function of θ. The finite-beam spectrum, obtained for a finite simply supported beams with 30 resonators, shows the presence of modes spanning the nontrivial gaps. The blue shaded area highlights the LR band gap, which is estimated according to the formula derived in Ref. [7]. (b) A detail of the spectrum showing four frequencies and corresponding bulk and edge-localized modes (the black curve represents the deflection of the beam, while the red circles denote the displacements of the resonators). (c) A detail of the spectrum showing three labeled nontrivial topological band gaps with an increasing number of topological modes (blue dashed lines separate regions between commensurate values of θ, while the blue shaded area highlights the region between $\theta = 2/30$ and $\theta = 3/30$). (d) The IDS as a function of θ exhibits sharp linear jumps at the band gaps. The slopes of three of these lines [highlighted by the white dashed lines and corresponding to the three gaps labeled in (c)] are equal to $m = 1, 2, 3$, while that for the LR band gap (highlighted by the red dashed line) is $m = 0$, which indicates that this band is topologically trivial.

gaps, which are topologically nontrivial, are crossed by several modes of the finite structure, the distinctive feature of which is their localized nature.

The enlarged spectrum of Fig. 2(b) compares selected modes corresponding, respectively, to the bulk and the finite-structure frequencies. Notably, the modes in the finite beam that appear in the band gap are edge localized at the right boundary ($x = L$). Also, the response of the resonators (shown in red circles) is of a localized nature when the beam's deflection is localized, while the relative displacements of the resonators are in phase and out of phase with respect to the beam at frequencies below and above the LR band gap, respectively. The fact that all of the modes spanning the nontrivial gaps are localized at the right boundary is a consequence of the way in which the finite beam is constructed from the pattern defined previously in Eq. (1). All finite beams are constructed by placing the first resonator at the space location at $x = a + R\sin(2\pi\theta)$ and adding resonators to the right boundary.

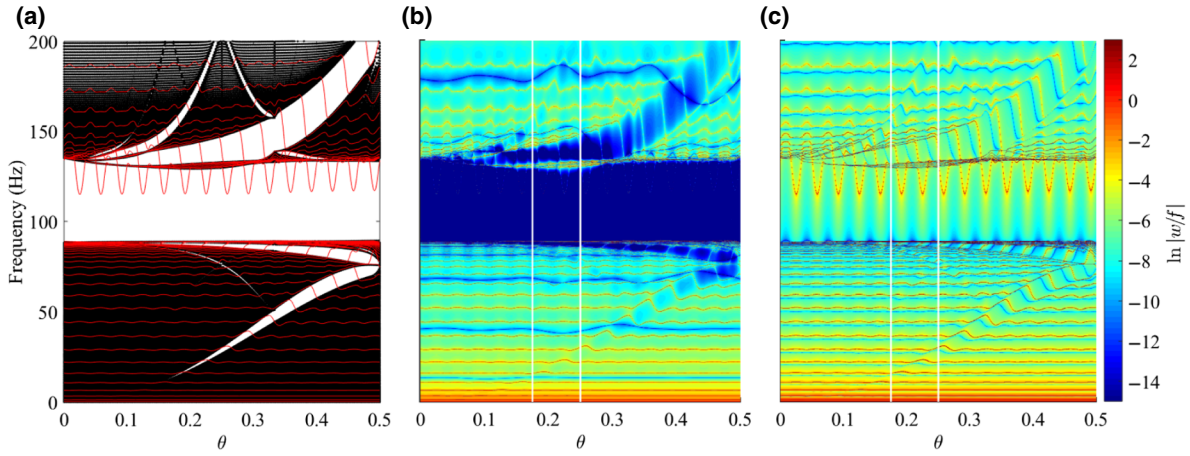

FIG. 3. (a) The bulk spectrum (black) and the finite spectrum for a clamped-free beam with 30 resonators (red). (b) The numerical frequency-response function of the beam spatially averaged between 20% and 30% of the beam span: the color map evolving from blue to red corresponds to the log scale of the magnitude. The blue regions highlight the low-response ranges corresponding to the band gaps. (c) The numerical frequency-response function of the beam spatially averaged between 90% and 100% of the beam span: the response near the beam tip highlights the presence of resonances within the gaps, which correspond to edge states. The vertical white lines in (b) and (c) correspond to the values of $\theta = 0.175$ and $\theta = 0.25$ considered in the experiments.

The existence of edge states can be predicted through the analysis of the topological properties of the bands, which are conveniently uncovered by estimating the integrated density of states (IDS) for the system [25,28]. Nontrivial gaps and the resulting onset of edge states spanning them are associated with changes in the IDS as θ varies. In the IDS representation of Fig. 2(d), a band gap appears as a line, the slope m of which indicates the number of topological boundary modes that span the band gap in the interval between two subsequent commensurate values of θ [28]. In this case, three IDS lines corresponding to the three topological band gaps [labeled in Fig. 2(c)] are shown as white dashed lines in Fig. 2(d), whereby $m = 1, 2, 3$, respectively, are the slopes of the corresponding gaps. The red dashed IDS line related to the LR band gap has a slope of $m = 0$, which indicates its topologically trivial nature and the lack of associated edge states spanning the gap [see Fig. 2(a)].

IV. NUMERICAL ANALYSES: A CANTILEVER BEAM

The finite system is implemented as a cantilever beam with clamped-free boundary conditions, with excitation applied at the free end. Numerical analyses (Fig. 3) are performed to evaluate the presence of the LR band gap and of additional gaps and to guide the selection of θ values for experimental investigation. On the finite structure, band gaps are conveniently visualized by evaluating the frequency-response function for the beam, averaged over a portion of the length. The choice of the portion of the beam to be averaged is driven by the need to show the response far from the excitation and not too close to the clamped boundary, so that the LR band gap, together with other additional topological band gaps, is visible in the averaged frequency response. For example, Fig. 3(b) shows the frequency response corresponding to the ratio of the

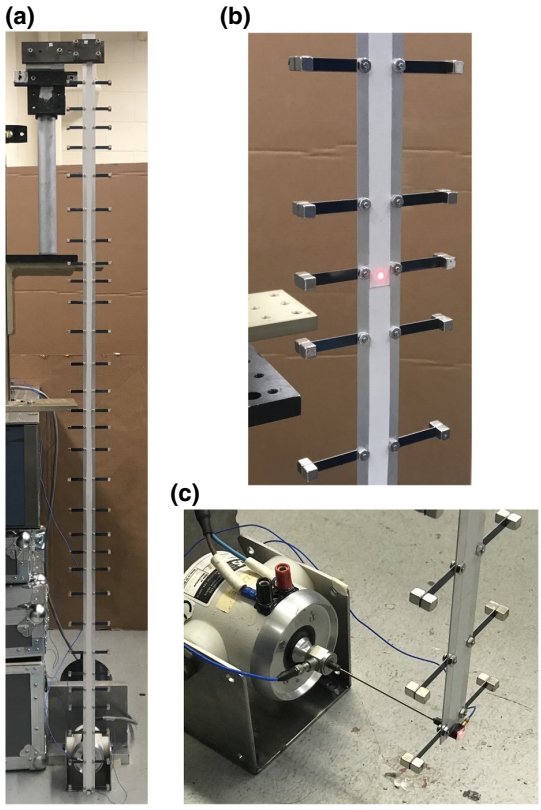

FIG. 4. The experimental setup, a cantilever beam with 30 resonators: (a) the front view of the beam; (b) a close-up of the resonators; and (c) view of the tip of the beam, excited by a electrodynamics shaker.

magnitude of the beam transverse deflection (output) to the magnitude of the input (forcing), averaged between 20% and 30% of the span from the clamped end. As a result, the color map in Fig. 3(b) is characterized by low-response regions (in blue) that highlight the attenuation occurring in the band gaps. This representation clearly outlines both the LR band gap and the additional topological gaps as θ varies. In contrast, Fig. 3(c), obtained by averaging the beam's response near the excitation, i.e., between 90% and 100% of the span, clearly highlights the modes of the finite systems, including the resonances localized in the gaps associated with the finite system. Of these modes, those in the LR gap are not topological and solely depend on the considered types of boundary conditions. Compared with the spectrum of the finite beam with simply supported boundaries on both ends [Fig. 2(a)], the spectrum of the clamped-free beam [Fig. 3(a)] has defect modes inside the trivial LR band gap. The nontrivial additional gaps are instead spanned by resonant modes as θ varies, regardless of the boundary conditions.

V. EXPERIMENTAL INVESTIGATIONS

For the experiments, $\theta = 0.175$ and $\theta = 0.25$ ensure a well-defined separation between the modes associated with the LR gap and the additional band gap. The selected two cases are highlighted by white lines in Figs. 3(b) and 3(c) for reference. The experimental investigations

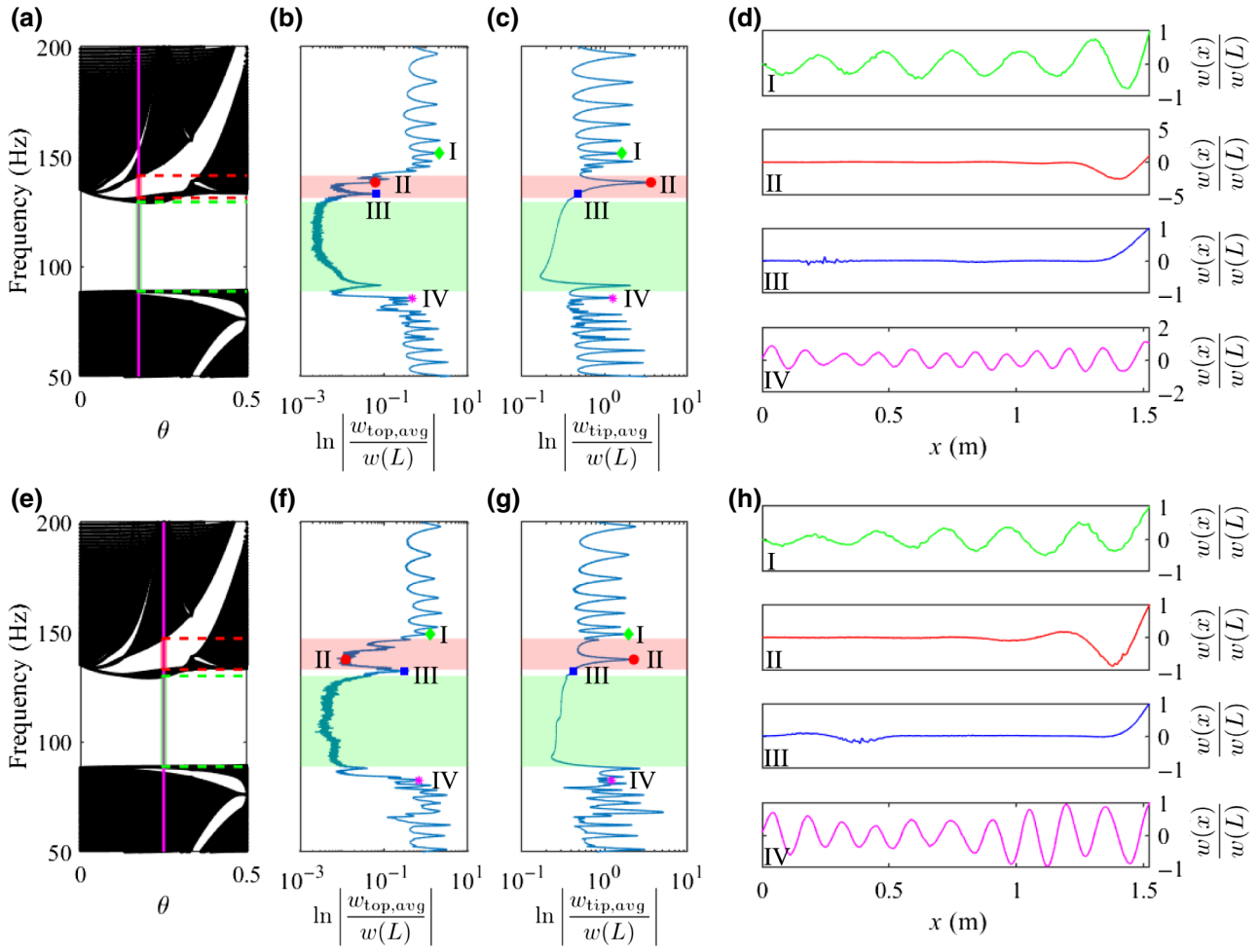

FIG. 5. (a),(e) Details of the numerical bulk spectrum, with vertical magenta lines corresponding to $\theta = 0.175$ and $\theta = 0.25$. The green and red dashed lines show the theoretical boundaries of the LR and nontrivial topological band gaps, respectively. (b)–(d) The experimental results for $\theta = 0.175$. (f)–(h) The experimental results for $\theta = 0.25$. The magnitude of the beam frequency response is spatially averaged between 20% and 30% (b),(f) and between 90% and 100% (c),(g) of the beam span. The green and red shaded areas highlight the theoretical LR and topological band gaps. (d),(h) The measured deflection shapes of the beam. Modes "I," "III," and "IV" are bulk modes at frequencies before the LR gap, between the LR and topological band gap, and after the topological band gap, respectively. The corresponding frequencies are marked by the green diamond, blue square, and magenta asterisk in (b), (c), (f), and (g). The mode labeled as "II" in (d) and (h) is edge localized, its frequency falls in the topologically nontrivial gap, and it is marked by a red circle in (c) and (g).

are presented to confirm the existence of the topologically nontrivial band gaps and the occurrence of edge-localized modes.

The finite system is physically implemented by employing a 1.524-m-long aluminum cantilever beam with 30 resonators (Fig. 4). Each resonator consists of a 8.26-cm-long strip of spring steel, which is 0.5 mm thick and 6.35 mm wide. Each strip is clamped symmetrically along the beam, thus forming two identical cantilevers. Two 6.35-mm^3 permanent magnets are placed at the tip of each cantilever, to add a tip mass of 3.6 g. The resulting natural frequency of each resonator is measured to be around 90 Hz. The beam is clamped vertically on one end and is excited by an electrodynamic shaker at the free end [Fig. 4(c)]. The force applied by the shaker is recorded by a force transducer, while the beam's velocity field is mapped by a scanning laser Doppler vibrometer (SLDV) over a grid of 158 points along the beam length (from the clamped boundary at top, $x = 0$, to the free end at bottom, $x = L$), which corresponds to a spatial resolution of 9.65 mm.

The experimental frequency response of the beam and the measured spatial distributions of selected operational deflection shapes are shown in Figs. 5(b)–5(d) for $\theta = 0.175$ and in Figs. 5(f)–5(g) for $\theta = 0.25$. The spatial distributions are normalized with respect to the displacements at the free end, $w(L)$. The LR band gap and the topological band gap are clearly observed from on the measured frequency response averaged between 20% and 30% of the beam span, i.e., away from the excitation location. Overall, the frequency location and frequency width of these bands agree well with the theoretical predictions shown as green and red shaded areas in Figs. 5(b) and 5(f). Both the center frequency and the width of the topological band gap increase as the QP pattern parameter θ varies from 0.175 to 0.25, which also agrees with the theoretical trend. Furthermore, the measured frequency response average near the free end, i.e., between 90% and 100% of the beam span, shows the presence of the localized modes that correspond to response peaks within the gap highlighted in Figs. 5(c) and 5(g). As expected from the theoretical predictions, the measured localized mode (red circle) for each case appears within the topological band gap and the localized nature at the edge is confirmed well by the corresponding operational deflection shape plotted in red and labeled "II" in Figs. 5(d) and 5(h). In addition, for each θ value considered, three bulk nonlocalized modes are also presented to illustrate their global deflection patterns. These modes are labeled "I," "III," and "IV" in the figure and their corresponding frequencies are part of the bulk spectrum in, respectively, the frequency range before the LR band gap, that between the LR and the topological band gap, and that after the topological band gap. It is to be noted that, unlike the cluster of several modes between LR band gap and the above additional nontrivial band gap shown in the simulations [Fig. 3(b)], the experimental measurements capture one distinguishable mode III (blue square), which can be due to the damping effect. The measured deflection shape of the beam at mode III has deflections at both the free end and close to the clamped boundary, hence confirming that it is a bulk mode.

VI. CONCLUSIONS

In conclusion, we investigate locally resonant metastructures in the form of beams with QP distributions of resonators. By varying the parameter θ defining the locations of the resonators, additional nontrivial topological band gaps are created. In finite metastructures, these bands host modes that are localized at the boundary and the frequency of which can be chosen through proper selection of the QP parameter defining the location of the resonators. The onset of the LR band gap and of the additional nontrivial band gaps with associated edge states is demonstrated through numerical simulations and in experiments conducted on a cantilever beam carrying an array of 30 resonators. The findings of the study suggest the application of QP placement of resonators or, in general, of mechanical inclusions, as a potentially effective way of achieving vibration attenuation over multiple subwavelength frequency bands. In addition, the ability to induce vibration localization at frequencies defined by the placement of resonating inclusions may find applications in vibration isolation and energy harvesting.

ACKNOWLEDGMENTS

We acknowledge funding support from the National Science Foundation through Emerging Frontiers in Research and Innovation (EFRI) program Grant No. 1741685 and from the Army Research Office through Grant No. W911NF-18-1-0036.

[1] Z. Liu, X. Zhang, Y. Mao, Y. Zhu, Z. Yang, C. T. Chan, and P. Sheng, Locally resonant sonic materials, Science **289**, 1734 (2000).

[2] D. Yu, Y. Liu, H. Zhao, G. Wang, and J. Qiu, Flexural vibration band gaps in Euler-Bernoulli beams with locally resonant structures with two degrees of freedom, Phys. Rev. B **73**, 064301 (2006).

[3] H. Sun, X. Du, and P. F. Pai, Theory of metamaterial beams for broadband vibration absorption, J. Intell. Mater. Syst. Struct. **21**, 1085 (2010).

[4] M. Oudich, M. Senesi, M. B. Assouar, M. Ruzenne, J.-H. Sun, B. Vincent, Z. Hou, and T.-T. Wu, Experimental evidence of locally resonant sonic band gap in two-dimensional phononic stubbed plates, Phys. Rev. B **84**, 165136 (2011).

[5] M. B. Assouar, M. Senesi, M. Oudich, M. Ruzzene, and Z. Hou, Broadband plate-type acoustic metamaterial for

low-frequency sound attenuation, Appl. Phys. Lett. **101**, 173505 (2012).
[6] R. Zhu, X. Liu, G. Hu, C. Sun, and G. Huang, A chiral elastic metamaterial beam for broadband vibration suppression, J. Sound Vib. **333**, 2759 (2014).
[7] C. Sugino, S. Leadenham, M. Ruzzene, and A. Erturk, On the mechanism of bandgap formation in locally resonant finite elastic metamaterials, J. Appl. Phys. **120**, 134501 (2016).
[8] D. Cardella, P. Celli, and S. Gonella, Manipulating waves by distilling frequencies: A tunable shunt-enabled rainbow trap, Smart Mater. Struct. **25**, 085017 (2016).
[9] P. Celli, B. Yousefzadeh, C. Daraio, and S. Gonella, Bandgap widening by disorder in rainbow metamaterials, Appl. Phys. Lett. **114**, 091903 (2019).
[10] C. Hodges, Confinement of vibration by structural irregularity, J. Sound Vib. **82**, 411 (1982).
[11] C. Hodges and J. Woodhouse, Vibration isolation from irregularity in a nearly periodic structure: Theory and measurements, J. Acoust. Soc. Am. **74**, 894 (1983).
[12] D. M. Photiadis and B. H. Houston, Anderson localization of vibration on a framed cylindrical shell, J. Acoust. Soc. Am. **106**, 1377 (1999).
[13] C. Pierre and E. Dowell, Localization of vibrations by structural irregularity, J. Sound Vib. **114**, 549 (1987).
[14] M. Z. Hasan and C. L. Kane, Colloquium: Topological insulators, Rev. Mod. Phys. **82**, 3045 (2010).
[15] L. Lu, J. D. Joannopoulos, and M. Soljačić, Topological photonics, Nat. Photonics **8**, 821 (2014).
[16] G. Ma, M. Xiao, and C. Chan, Topological phases in acoustic and mechanical systems, Nat. Rev. Phys. **1**, 281 (2019).
[17] Y. Kraus, Y. Lahini, Z. Ringel, M. Verbin, and O. Zilberberg, Topological States and Adiabatic Pumping in Quasicrystals, Phys. Rev. Lett. **109**, 106402 (2012).
[18] Y. Kraus and O. Zilberberg, Quasiperiodicity and topology transcend dimensions, Nat. Phys. **12**, 624 (2016).
[19] K. Madsen, E. Bergholtz, and P. Brouwer, Topological equivalence of crystal and quasicrystal band structures, Phys. Rev. B **88**, 125118 (2013).
[20] T. Ozawa, H. M. Price, N. Goldman, O. Zilberberg, and I. Carusotto, Synthetic dimensions in integrated photonics: From optical isolation to four-dimensional quantum Hall physics, Phys. Rev. A **93**, 043827 (2016).
[21] D.-T. Tran, A. Dauphin, N. Goldman, and P. Gaspard, Topological Hofstadter insulators in a two-dimensional quasicrystal, Phys. Rev. B **91**, 085125 (2015).
[22] E. Prodan, Virtual topological insulators with real quantized physics, Phys. Rev. B **91**, 245104 (2015).
[23] L. Morini and M. Gei, Waves in one-dimensional quasicrystalline structures: Dynamical trace mapping, scaling and self-similarity of the spectrum, J. Mech. Phys. Solids **119**, 83 (2018).
[24] M. Gei, Wave propagation in quasiperiodic structures: Stop/pass band distribution and prestress effects, Int. J. Solids Struct. **47**, 3067 (2010).
[25] D. J. Apigo, K. Qian, C. Prodan, and E. Prodan, Topological edge modes by smart patterning, Phys. Rev. Mater. **2**, 124203 (2018).
[26] D. J. Apigo, W. Cheng, K. F. Dobiszewski, E. Prodan, and C. Prodan, Observation of Topological Edge Modes in a Quasiperiodic Acoustic Waveguide, Phys. Rev. Lett. **122**, 095501 (2019).
[27] X. Ni, K. Chen, M. Weiner, D. J. Apigo, C. Prodan, A. Alù, E. Prodan, and A. B. Khanikaev, Observation of Hofstadter butterfly and topological edge states in reconfigurable quasi-periodic acoustic crystals, Commun. Phys. **2**, 55 (2019).
[28] R. K. Pal, M. I. Rosa, and M. Ruzzene, Topological bands and localized vibration modes in quasiperiodic beams, arXiv:1906.00151 (2019).
[29] D. R. Hofstadter, Energy levels and wave functions of Bloch electrons in rational and irrational magnetic fields, Phys. Rev. B **14**, 2239 (1976).